Electronic Supplementary Material (ESI) for Chemical Science.

A comparative study of the coordination behavior of cyclo-P_5 and cyclo-As_5 ligand complexes towards the trinuclear Lewis acid complex (perfluoro-ortho-phenylene)mercury

Martin Fleischmann,[a] James Jones,[b] François Gabbaï,[b] Manfred Scheer[a]*

[a] Institut für Anorganische Chemie, Universität Regensburg, 93040 Regensburg, Germany, manfred.scheer@chemie.uni-regensburg.de
Fax: (+49) 941-943-4439
[b] Department of Chemistry, Texas A&M University, College Station, Texas 77843-3255, USA

Contents

1 General information

All experiments were performed under an atmosphere of dry argon or nitrogen using standard Schlenk and drybox techniques. Commercially available reagents were used as received without further purification. Solvents were freshly distilled under nitrogen from CaH_2 (CH_2Cl_2, CD_2Cl_2), Solution NMR spectra were recorded on a Bruker Avance 400 spectrometer (^{1}H: 400.130 MHz, ^{31}P: 161.976 MHz, ^{13}C: 100.613 MHz). The chemical shifts δ are presented in parts per million ppm and coupling constants J in Hz. The following samples were used for external reference: TMS (^{1}H, ^{13}C), $CFCl_3$ (^{19}F), H_3PO_4 85 % (^{31}P). IR spectra were recorded on a VARIAN FTS-800 FT-IR spectrometer. The solid substances were grinded together with dried KBr and pressed to pellets. The starting materials **1, 2** and **3** were prepared according to the literature procedure.[1]

2 Syntheses of the compound 6 a-c:

The preparation of the starting *cyclo*-P_5 sandwich complexes is easily done following the same procedure as it was done for the Cp* analogues complex. Table 1 shows the quantities and yields for the different reactions.

Procedure: Solid P_4 is weighed into a round bottom flask together with solid $[Cp^RFe(CO)_2]_2$ and decalin is added. The resulting mixture was refluxed for 3 h. During this time a color change from dark red to olive green to dark brown is observed. The solvent is evaporated under reduced pressure. The solid remainder was dissolved in a small amount of CH_2Cl_2, some silica gel added and the solvent removed until a free flowing brown powder remained. Column chromatographic workup on silica with pure *n*-hexane afforded only a green band. Other side products were not isolated for this work. The green solution was reduced to a minimum and stored at –30 °C. After one day **6 a** and **6 c** form dark green blocks but **6 b** can only be isolated as a light green powder. The mother liquor is removed and the crystals dried in vacuum. To grow crystals of **6 b**, a saturated solution in Et_2O at room temperature was cooled to –30 °C.

Table 1. Summary of the quantities used for the preparation of 6 a-c;

	$m([Cp^RFe(CO)_2]_2)$/g	$n([Cp^RFe(CO)_2]_2)$/mmol	$m(P_4)$/g	$n(P_4)$/mmol	V(decalin)/mL	Yield/g	in %
Cp'FeP5	3.8	8.2	4.1	33.1	200	0.46	8.5
Cp''FeP5	5.2	9.0	5.0	40.4	200	2.34	33.5
Cp'''FeP5	0.28	0.40	0.30	2.42	50	0.16	45

3 Analytical data for 6 a-c:

3.1 [Cp'Fe(η^5-P_5)] (6 a):

Yield	460 mg (8.5 %)
^{1}H-NMR (C_6D_6)	δ/ppm = 0.89 (s, Me, 9H), 3.41 (s, CpH, 2H), 3.55 (s, CpH, 2H)
^{13}C{^{1}H}-NMR (C_6D_6)	δ/ppm = 30.05 (s, Me), 31.05 (s, CMe3), 73.72 (s, CpH), 65.20 (s, CpH), 110.87 (s, Cp^{t}Bu)
^{31}P{^{1}H}-NMR (C_6D_6)	δ/ppm = 168.20 (s, P_5)
EI-MS (CH_2Cl_2)	m/z (%) = 331.9 (100) $[Cp'FeP_5]^+$, 269.9 (82) $[Cp'FeP_3]^+$

IR (KBr)	$\tilde{\nu}$/cm^{-1} = 3089 (w), 2956 (m), 2927 (w), 2898 (w), 2861 (w), 1480 (m), 1456 (w), 1396 (m), 1361 (m), 1273 (w), 1149 (w), 1037 (w), 905 (w), 842 (m)
Elemental analysis:	calc for [$C_9H_{13}FeP_5$] C: 32.57 %, H: 3.95 %, found C: 32.52 %, H: 3.98 %

3.2 [Cp''Fe(η^5-P_5)] (6 b):

Yield	2.34 g (33.5 %)
^{1}H-NMR (C_6D_6)	δ/ppm = 1.01 (s, Me, 18H), 3.63 (s, CpH, 2H), 3.65 (s, CpH, 1H)
^{13}C{^{1}H}-NMR (C_6D_6)	δ/ppm = 30.36 (s, Me), 31.52 (s, CMe_3), 70.34 (s, CpH), 72.10 (s, CpH), 109.79 (s, Cp^{t}Bu)
^{31}P{^{1}H}-NMR (C_6D_6)	δ/ppm = 166.44 (s, P_5)
^{31}P-NMR (C_6D_6)	δ/ppm = 166.43 (s, P_5)
EI-MS (CH_2Cl_2)	*m/z* (%) = 388.0 (100) [Cp''FeP_5]$^+$, 326.0 (98) [Cp''FeP_3]$^+$
IR (KBr)	$\tilde{\nu}$/cm^{-1} = 2957 (m), 2927 (vw), 2900 (w), 2862 (w), 1486 (w), 1458 (w), 1367 (w), 1360 (m), 1251 (w), 1163 (w), 1051 (w), 863 (m), 845 (m)

3.3 [Cp'''Fe(η^5-P_5)] (6 c):

Yield	160 mg (45 %)
^{1}H-NMR (C_6D_6)	δ/ppm = 1.08 (s, Me, 9H), 1.20 (s, Me, 18H), 3.95 (s, CpH, 2H)
^{13}C{^{1}H}-NMR (C_6D_6)	δ/ppm = 30.57 (m, Me), 31.62 (s, CMe_3), 33.28 (s, CMe_3), 33.42 (m, Me), 73.10 (s, CpH), 104.60 (s, Cp^{t}Bu), 106.66 (s, Cp^{t}Bu)
^{31}P{^{1}H}-NMR (C_6D_6)	δ/ppm = 165.24 (s, P_5)
EI-MS:	m/z (%): 444.0/100% ($M^{+\cdot}$), 382.0/65% (-P_2), 386.9/12% (M–C_4H_9)
Elemental analysis:	calc for [$C_{17}H_{29}FeP_5$] C: 45.97 %; H 6.58 % found C: 45.96 %, H: 6.53 %
EI-MS (CH_2Cl_2)	*m/z* (%) = 444.0 (100) [Cp'''FeP_5]$^+$, 382.0 (65) [Cp'''FeP_3]$^+$, 386.9 (12) [$C_{13}H_{20}FeP_5$]$^+$
IR (KBr)	$\tilde{\nu}$/cm^{-1} = 2957 (m), 2920 (w), 2864 (w), 1491 (vw), 1460 (vw), 1363 (w), 1247 (vw), 1169 (vw), 1020 (vw)

4 Syntheses of the compounds 4, 5 and 7 a-c:

Since CH_2Cl_2 is considered as a very weak donor, the reactions were performed in this solvent. Furthermore, all used *cyclo*-E_5 ligand complexes and also the Lewis acid [(*o*-$C_6F_4Hg)_3$] show a good solubility in CH_2Cl_2.

For the preparation of the compounds **4**, **5** and **7 a-c**, the *cyclo*-E_5 ligand complexes were weighed together with solid [(*o*-$C_6F_4Hg)_3$]. The used amounts for all reactions can be found in Table 2. CH_2Cl_2 was added while stirring the reaction until the solution turned clear (about 10 to 20 mL). This solution was filtered into another flask and the solvent was slowly evaporated while stirring. The solid that forms above the solvent was repeatedly dissolved again. When the solid starts to dissolve only very slowly, the solution is warmed to room temperature. When the solution is completely clear again, the flask is stored at +4 °C or –30 °C. The crystals usually form on the walls of the flask above the solvent at +4 °C or inside the solution at –30 °C.

Table 2. Summary of the quantities used for the preparation of compounds 4, 5, and 7 a-c;

Complex	$m(Cp^RFeE_5)$/mg	$n(Cp^RFeE_5)$/mmol	$m(Hg_3C_{18}F_{12})$/mg	$n(Hg_3C_{18}F_{12})$/mmol	Yield/mg	in %
Cp^*FeP_5	35	0.1	105	0.1	87	62
Cp^*FeAs_5	57	0.1	105	0.1	124	77
$Cp'FeP_5$	33	0.1	105	0.1	67	49
$Cp''FeP_5$	39	0.1	105	0.1	76	53
$Cp'''FeP_5$	45	0.1	105	0.1	94	63

5 Analytical data for the compounds 4, 5, 7a-c:

5.1 $[\{Cp^*Fe(\eta^5\text{-}P_5)\}\bullet\{(o\text{-}C_6F_4Hg)_3\}]$ (4)

Yield	87 mg (62 %)
^{1}**H-NMR** (CD_2Cl_2)	δ/ppm = 1.38 (s, Cp*)
^{13}**C{^{1}H}-NMR** (CD_2Cl_2)	δ/ppm = 91.93 (s, C_{Cp}), 10.95 (s, CH_3)
^{19}**F-NMR** (CD_2Cl_2)	δ/ppm = –120.66 (m, *o*-F), –155.34 (m, *p*-F)
^{31}**P{^{1}H}-NMR** (CD_2Cl_2)	δ/ppm = 155.32 (s, P_5)
^{31}**P-NMR** (CD_2Cl_2)	δ/ppm = 155.32 (s, P_5)
FD-MS (CH_2Cl_2)	*m/z* (%) = 346.1 (100) $[Cp^*FeP_5]^+$, 1046.3 (50) $[Hg_3C_{18}F_{12}]^+$
IR (KBr)	$\tilde{\nu}$/cm^{-1} = 2978 (vw), 2959 (vw), 2909 (vw), 1616 (w), 1583 (w), 1475 (vs), 1419 (s), 1377 (w), 1289 (m), 1088 (m), 1005 (m), 816 (w)
Elemental analysis:	calc for $[Hg_3C_{18}F_{12}][C_{10}H_{15}FeP_5]$ C: 24.16 %, H: 1.09 %, found C: 24.18 %, H: 1.10 %

NMR spectra at different temperatures for compound 4

^{1}**H-NMR** (CD_2Cl_2, 300 K)	δ/ppm = 1.39 (s, CH_3)
^{1}**H-NMR** (CD_2Cl_2, 193 K)	δ/ppm = 1.22 (s, CH_3)
^{31}**P-NMR** (CD_2Cl_2, 300 K)	δ/ppm = 154.8 (s, P_5)
^{31}**P-NMR** (CD_2Cl_2, 193 K)	δ/ppm = 156.7 (s, P_5)

NMR spectra at different temperatures for the free ligand compex 1

^{1}**H-NMR** (CD_2Cl_2, 300 K)	δ/ppm = 1.43 (s, CH_3)
^{1}**H-NMR** (CD_2Cl_2, 193 K)	δ/ppm = 1.35 (s, CH_3)
^{31}**P-NMR** (CD_2Cl_2, 300 K)	δ/ppm = 152.3 (s, P_5)
^{31}**P-NMR** (CD_2Cl_2, 193 K)	δ/ppm = 149.1 (s, P_5)

5.2 $[\{Cp^*Fe(\eta^5\text{-}As_5)\}\bullet\{(o\text{-}C_6F_4Hg)_3\}]$ (5)

Yield	124 mg (77 %)
^{1}**H-NMR** (CD_2Cl_2)	δ/ppm = 1.27 (s, Cp*)
^{13}**C{^{1}H}-NMR** (CD_2Cl_2)	δ/ppm = 12.12 (s, Me), 88.75 (s, Cp)
^{19}**F-NMR** (CD_2Cl_2)	δ/ppm = –120.64 (m, *o*-F), –155.80 (m, *p*-F)
FD-MS (CH_2Cl_2)	*m/z* (%) = 566.0 (18) $[Cp^*FeAs_5]^+$, 756.8 (100) $[Cp^*_2Fe_2As_5]^+$, 1045.8 (8) $[Hg_3C_{18}F_{12}]^+$
IR (KBr)	$\tilde{\nu}$/cm^{-1} = 2963 (vw), 2910 (vw), 2858 (vw), 1614 (w), 1581 (w), 1472 (vs), 1417 (s), 1376 (w), 1287 (w), 1086 (m), 1004 (m), 814 (w)

Elemental analysis:	calc for [$C_{10}H_{15}FeAs_5$•$Hg_3C_{18}F_{12}$] C: 20.87 %, H: 0.94 %, found C: 20.89 %, H: 0.98 %

5.3 [{Cp'Fe(η^5-P_5)}•{(*o*-C_6F_4Hg)$_3$}] (7 a)

Yield	67 mg (49 %)
^{1}H-NMR (CD_2Cl_2)	δ/ppm = 1.13 (s, Me, 9H), 4.06 (s, CpH, 2H), 4.21 (s, CpH, 2H)
^{19}F-NMR (CD_2Cl_2)	δ/ppm = –120.77 (m, *o*-F), –155.10 (m, *p*-F)
^{31}P{^{1}H}-NMR (CD_2Cl_2)	δ/ppm = 168.70 (s, P_5)
FD-MS (CH_2Cl_2)	*m/z* (%) = 332.0 (100) [Cp'FeP5]$^+$, 1046.9 (8) [$Hg_3C_{18}F_{12}$]$^+$
IR (KBr)	$\tilde{\nu}$/cm^{-1} = 3118 (vw), 2965 (w), 2955 (w), 2934 (vw), 2927 (w), 2906 (vw), 2868 (vw), 1615 (m), 1583 (m), 1471 (vs), 1420 (s), 1288 (s), 1252 (m), 1088 (s), 1004 (s), 850 (m), 814 (m), 771 (m)
Elemental analysis:	calc for [$Hg_3C_{18}F_{12}$][$C_9H_{13}FeP_5$] C: 23.54 %, H: 0.95 %, found C: 23.97 %, H: 1.16 %

5.4 [{Cp''Fe(η^5-P_5)}•{(*o*-C_6F_4Hg)$_3$}] (7 b)

Yield	76 mg (53 %)
^{1}H-NMR (CD_2Cl_2)	δ/ppm = 1.16 (s, Me, 18H), 3.90 (s, CpH, 1H), 4.05 (s, CpH, 2H)
^{19}F-NMR (CD_2Cl_2)	δ/ppm = –120.75 (m, *o*-F), –155.10 (m, *p*-F)
^{31}P{^{1}H}-NMR (CD_2Cl_2)	δ/ppm = 166.94 (s, P_5)
FD-MS (CH_2Cl_2)	*m/z* (%) = 388.1 (100) [Cp''FeP_5]$^+$, 1045.9 (30) [$Hg_3C_{18}F_{12}$]$^+$
IR (KBr)	$\tilde{\nu}$/cm^{-1} = 2968 (w), 2959 (w), 2905 (vw), 2864 (vw), 1616 (w), 1582 (w), 1473 (vs), 1418 (s), 1289 (m), 1085 (m), 1006 (m), 814 (w)
Elemental analysis:	calc for [$Hg_3C_{18}F_{12}$][$C_{13}H_{21}FeP_5$] C: 25.97 %, H: 1.48 %, found C: 26.10 %, H: 1.58 %

5.5 [{Cp'''Fe(η^5-P_5)}•{(*o*-C_6F_4Hg)$_3$}] (7 c)

Yield	94 mg (63 %)
^{1}H-NMR (CD_2Cl_2)	δ/ppm = 1.17 (s, Me, 9H), 1.31 (s, Me, 18H), 4.08 (s, CpH, 2H)
^{19}F-NMR (CD_2Cl_2)	δ/ppm = –120.73 (m, *o*-F), –155.19 (m, *p*-F)
^{31}P{^{1}H}-NMR (CD_2Cl_2)	δ/ppm = 166.38 (s, P_5)
FD-MS (CH_2Cl_2)	*m/z* (%) = 444.2 (100) [Cp'''FeP5]$^+$, 1046.1 (28) [$Hg_3C_{18}F_{12}$]$^+$
IR (KBr)	$\tilde{\nu}$/cm^{-1} = 2965 (w), 2927 (vw), 2872 (vw), 1615 (vw), 1583 (vw), 1471 (vs), 1418 (s), 1289 (m), 1250 (w), 1082 (m), 1005(m), 815 (w), 770 (vw)
Elemental analysis:	calc for [$Hg_3C_{18}F_{12}$][$C_{17}H_{29}FeP_5$] C: 28.21 %, H: 1.96 %, found C: 28.79 %, H: 2.13 %

6 Crystal structure of [{(*o*-C_6F_4Hg)$_3$}•{Cp*Fe(η^5-As_5)}$_2$]•[Cp*Fe(η^5-As_5)]•(toluene) (8)

When the *cyclo*-As_5 complex **2** was combined with [(*o*-C_6F_4Hg)$_3$] in CH_2Cl_2 in a small tube which was stored for several weeks in a closed jar with some toluene for gas phase diffusion, it was possible to isolate and analyze some crystals of the novel adduct **8**. Compound **8** crystallizes in the monoclinic space group *C*2/*c*. The asymmetric unit contains Three independent *cyclo*-As_5 sandwich complexes, one molecule of [(*o*-C_6F_4Hg)$_3$] and one and a half toluene molecules. Figure 1 shows the solid state structure of **8**. The As_5 ring As11-As15 is disordered over three positions with the occupancies of 53:28:19. Only the major part is shown here. Unfortunately, we were not able to reproduce this result in a selective manner. Nevertheless, the solid state structure will be presented since it shows the preference of the weak Hg-As interactions over the interactions of **3** with the electron rich toluene molecules which are also found in the crystal lattice.

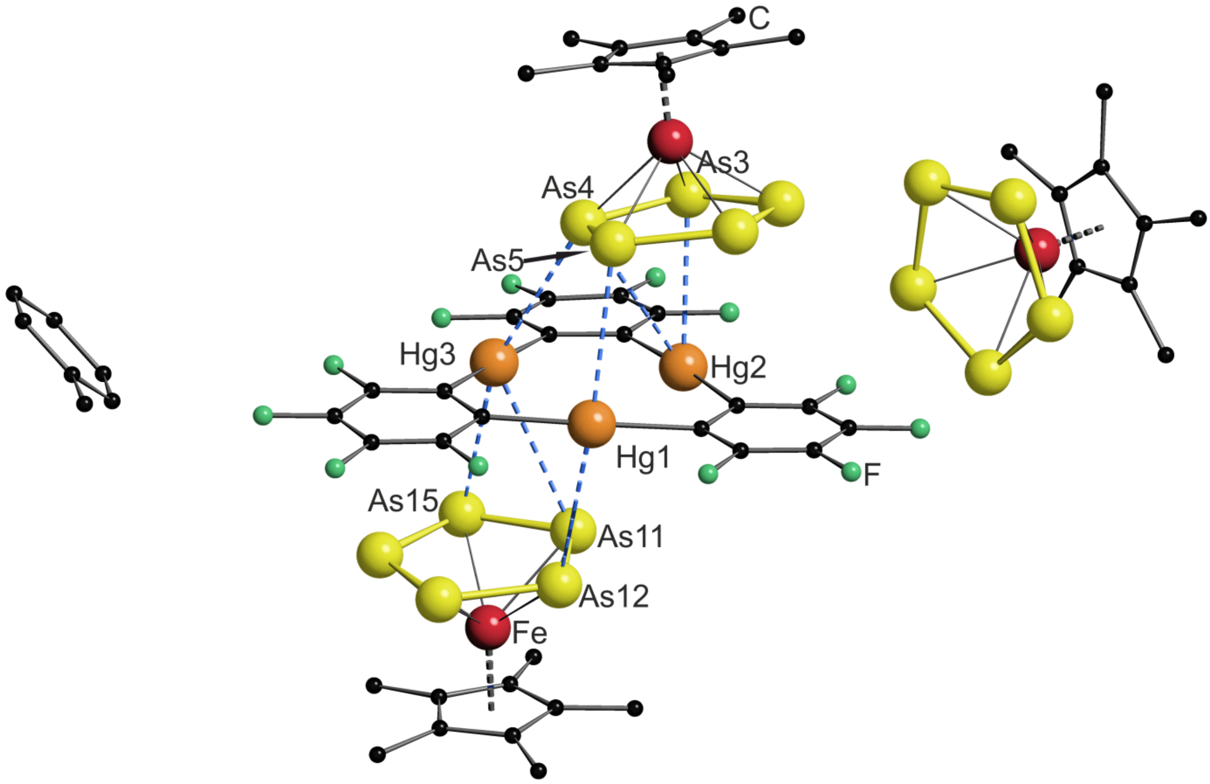

Figure 1. Solid state structure of 8; The toluene molecule on the left and the pentaarsaferrocene molecule on the right show no short contacts to [(*o*-C_6F_4Hg)$_3$]. The As5 ring As11-As15 is disordered over three positions while only the major part is depicted here (53 % occupancy). Selected bond lengths [Å] and angles [°]: Hg1-As5 3.5329(7), Hg1-As12 3.579(5), Hg2-As3 3.2846(6), Hg2-As4 3.6852(5), Hg3-As4 3.4738(7), Hg3-As11 3.641(7) Hg3-As15 3.486(8), angle (As1-As5 plane to Hg_3 plane) 12.07(1), angle (As11-As15 plane to Hg_3 plane) 6.45(9).

7 CH_2Cl_2 solvates of [(*o*-C_6F_4Hg)$_3$]: X-ray of [{(*o*-C_6F_4Hg)$_3$}•CH_2Cl_2] (9)

In another unrelated reaction, we were able to identify crystals of the CH_2Cl_2 solvate of the Lewis acid **3**. This result was surprising since no adduct of CH_2Cl_2 and **3** was either expected or reported so far, since the CH_2Cl_2 is supposed to be a very weak donor. Compound **9** crystallizes in the triclinic space group *P*-1. The asymmetric unit contains one molecule of [(*o*-C_6F_4Hg)$_3$] and one CH_2Cl_2 molecule. Figure 2 shows the solid state structure of **9**. The solvent molecule is not disordered. There is a short contact of Cl2 to Hg1 of 3.351(2) Å that is considerably shorter than the sum of the vdW radii for Hg and Cl (3.5 Å).

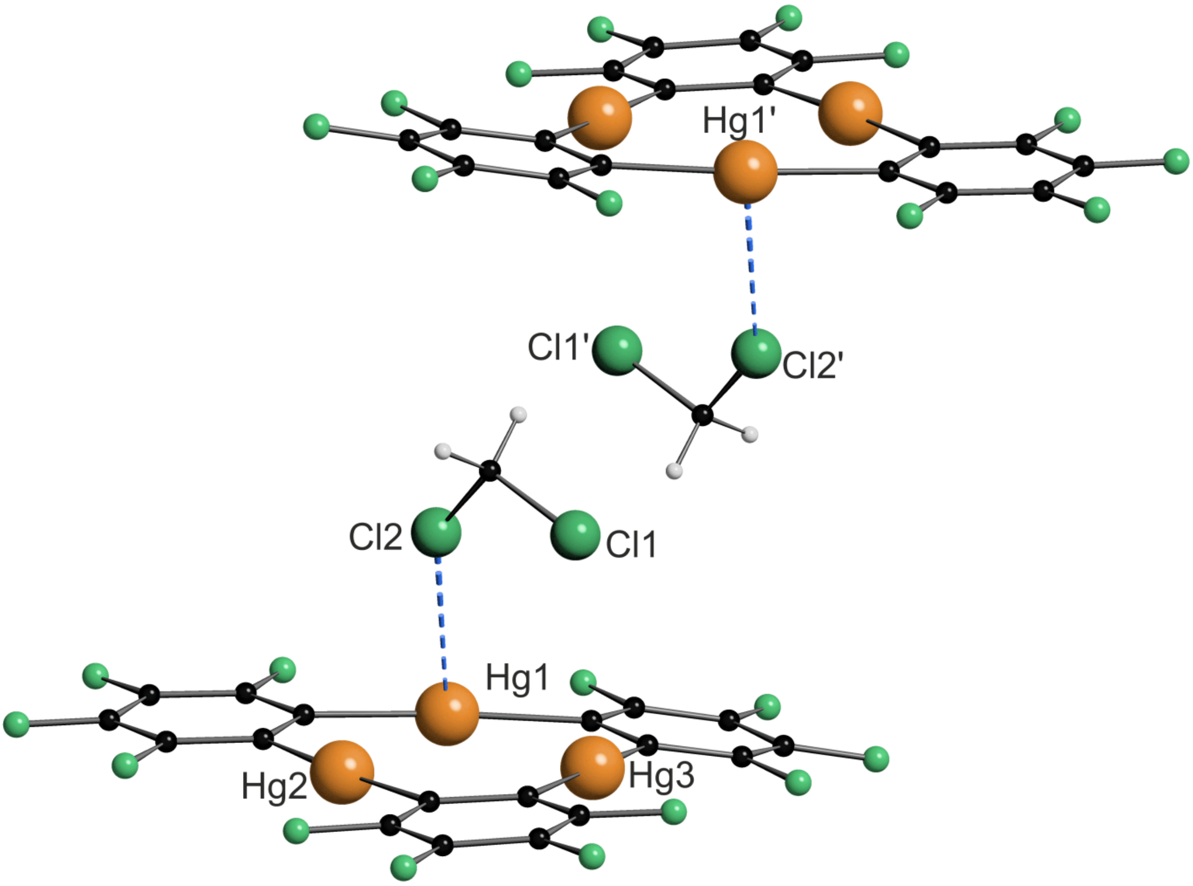

Figure 2. Solid state structure of compound 9; Hg1-Cl2 3.351(2).

Additional unit cell for a CH_2Cl_2 solvate of $[(o\text{-}C_6F_4Hg)_3]$

In addition to the compound **9** another sort of crystals that only contain $[(o\text{-}C_6F_4Hg)_3]$ and CH_2Cl_2 could be obtained from an unrelated reaction. Unfortunately, in this case the solvent molecules as well as one $[(o\text{-}C_6F_4Hg)_3]$ molecule are severely disordered and no satisfactory structure solution could be obtained. Therefore, we just report the unit cell for future reference.

Table 3. Unit cell of a second CH_2Cl_2 solvate of $[(o\text{-}C_6F_4Hg)_3]$

crystal system	triclinic	α [°]	60.940(7)
a [Å]	12.5016(7)	β [°]	81.802(6)
b [Å]	14.1313(10)	γ [°]	87.573(5)
c [Å]	14.2267(11)	V [Å^3]	2173.4(2)

8 X-ray diffraction analysis

All diffraction experiments were performed at 123 K. The different data sets were either collected on an Agilent Gemini R Ultra diffractometer with Cu-K_α or Mo-K_α radiation or an Agilent SuperNova diffractometer with Cu-K_α radiation. Crystallographic data together with the details of the experiments are given in the Tables 4 and 5. All crystal preparations were performed under mineral oil. The cell determination, data reduction and absorption correction for all other compounds were performed with the help of the CrysAlis PRO software by Agilent Technologies Ltd.[2] The structure solution was done by direct methods with SIR97[3] or ShelXS.[4] The full-matrix least-square refinement against F^2 was done with ShelXL.[4] All fully occupied atoms except hydrogen were refined anisotropically. The H atoms were calculated geometrically and a riding model was used during the refinement process. Graphical material was created with the free software Schakal99.[5]

CCDC-1012615-1012624 contain the supplementary crystallographic data for this paper. These data can be obtained free of charge from the Cambridge Crystallographic Data Centre via www.ccdc.cam.ac.uk/data_request/cif.

Table 4. Crystallographic data for the compounds 4, 5 and 6a-c.

	4	**5**	**6a**	**6b**	**6c**
Empirical formula	$C_{29}H_{17}Cl_2F_{12}FeHg_3P_5$	$C_{29}H_{17}As_5Cl_2F_{12}FeHg_3$	$C_9H_{13}FeP_5$	$C_{13}H_{21}FeP_5$	$C_{17}H_{29}FeP_5$
M [gmol^{-1}]	1476.80	1696.55	331.89	388.00	444.10
Crystal size [mm]	0.19 × 0.12 × 0.10	0.24 × 0.10 × 0.05	0.28 × 0.19 × 0.09	0.28 × 0.07 × 0.06	0.29 × 0.24 × 0.16
T [K]	123(1)	123(1)	123(1)	123(1)	123(1)
λ [Å]	0.71073	0.71073	1.54178	1.54178	0.71073
crystal system	Triclinic	Triclinic	orthorhombic	orthorhombic	monoclinic
space group	$P\bar{1}$	$P\bar{1}$	$Pnma$	$Pca2_1$	$P2_1/c$
a [Å]	11.7330(2)	11.9982(2)	11.4347(1)	18.7588(8)	9.0507(1)
b [Å]	12.1852(2)	13.3448(2)	23.4865(2)	6.5778(3)	25.6020(3)
c [Å]	13.1641(2)	14.1016(2)	15.1315(1)	14.1509(6)	10.1648(2)
α [°]	85.129(1)	65.329(1)	90	90	90
β [°]	80.243(1)	78.072(1)	90	90	115.783(2)
γ [°]	74.103(2)	66.415(2)	90	90	90
V [Å^3]	1782.43(5)	1878.24(6)	4063.73(6)	1746.10(13)	2120.87(6)
Z	2	2	12	4	4
ρ_{calc} [gcm^{-3}]	2.752	3.000	1.628	1.476	1.391
μ [mm^{-1}]	13.702	17.197	14.256	11.129	1.085
diffractometer	Agilent Gemini R Ultra	Agilent Gemini R Ultra	Agilent SuperNova	Agilent Gemini R Ultra	Agilent Gemini R Ultra
radiation	Mo–K_{α}	Mo–K_{α}	Cu–K_{α}	Cu–K_{α}	Mo–K_{α}
θ range [°]	3.14 – 27.10	3.00 – 27.48	3.47 – 73.60	4.71 – 67.00	2.96 – 27.00
absorption correct.	analytical	Analytical	analytical	analytical	analytical
T_{min} / T_{max}	0.170 / 0.381	0.070 / 0.456	0.081 / 0.391	0.115 / 0.587	0.794 / 0.875
reflns collect / unique	43547 / 7854	22941 / 8567	41579 / 4180	3376 / 2274	35725 / 5783
reflns obs [I>2$\sigma(I)$]	6612	6941	4068	1847	4883
R_{int}	0.0362	0.0292	0.0568	0.0380	0.0264
Flack parameter	—	—	—	0.025(8)	—
parameters / restraints	474 / 0	474 / 0	211 / 0	249 / 33	217 / 0
GOF on F^2	0.897	0.935	1.063	0.950	1.059
R_1 / wR_2 [I>2 $\sigma(I)$]	0.0170 / 0.0307	0.0200 / 0.0394	0.0213 / 0.0541	0.0427 / 0.0910	0.0230 / 0.0609
R_1 / wR_2 (all data)	0.0223 / 0.0311	0.0272 / 0.0400	0.0225 / 0.0549	0.0510 / 0.0929	0.0283 / 0.0618
max / min $\Delta\rho$[eÅ^{-3}]	0.738 / –0.936	1.149 / –0.993	0.301 / –0.356	0.352 / –0.556	0.360 / –0.295

Table 5. Crystallographic data for the compounds 7a-c, 8 and 9.

	7a	**7b**	**7c**	**8**	**9**
Empirical formula	$C_{28}H_{15}Cl_2F_{12}FeHg_3P_5$	$C_{31}H_{21}F_{12}FeHg_3P_5$	$C_{73}H_{64}Cl_6F_{24}Fe_2Hg_6P_{10}$	$C_{55}H_{53}As_{15}F_{12}Fe_3Hg_3$	$C_{19}H_2Cl_2F_{12}Hg_3$
M [gmol^{-1}]	1462.77	1433.95	3234.88	2835.09	1130.88
Crystal size [mm]	0.41 × 0.28 × 0.16	0.42 × 0.18 × 0.11	0.26 × 0.20 × 0.16	0.29 × 0.09 × 0.05	0.25 × 0.10 × 0.06
T [K]	123(1)	123(1)	123(1)	123(1)	123(1)
λ [Å]	0.71073	0.71073	0.71073	0.71073	0.71073
crystal system	triclinic	triclinic	monoclinic	monoclinic	triclinic
space group	$P\bar{1}$	$P\bar{1}$	$P2_1$	$C2/c$	$P\bar{1}$
a [Å]	11.6373(4)	12.0744(2)	12.3145(3)	48.2155(11)	9.2776(2)
b [Å]	11.8015(3)	12.2486(2)	26.4751(6)	14.1380(2)	9.7199(2)
c [Å]	15.7005(5)	14.5238(3)	14.4338(3)	22.3159(5)	12.7689(2)
α [°]	89.754(2)	69.244(2)	90	90	103.463(1)
β [°]	68.252(3)	82.395(2)	107.168(2)	109.887(2)	100.800(2)
γ [°]	66.286(3)	65.440(2)	90	90	97.447(2)
V [Å^3]	1806.94(12)	1826.58(7)	4496.14(18)	14304.9(5)	1081.75(4)
Z	2	2	2	8	2
ρ_{calc} [gcm^{-3}]	2.688	2.607	2.389	2.633	3.472
μ [mm^{-1}]	13.551	13.261	10.963	13.914	21.239
diffractometer	Agilent Gemini R Ultra	Agilent Gemini R Ultra	Agilent Gemini R Ultra	Agilent Gemini R Ultra	Agilent Gemini R Ultra
radiation	Mo–K_{α}	Mo–K_{α}	Mo–K_{α}	Mo–K_{α}	Mo–K_{α}
θ range [°]	2.96 – 27.00	2.90 – 30.11	2.74 – 27.10	2.81 – 27.48	2.86 – 28.50
absorption correct.	analytical	Analytical	Analytical	analytical	analytical
T_{min} / T_{max}	0.081 / 0.243	0.034 / 0.400	0.136 / 0.369	0.129 / 0.510	0.081 / 0.403
reflns collect / unique	12948 / 8836	43916 / 9760	39551 / 19613	39165 / 15949	42673 / 6017
reflns obs [I>2$\sigma(I)$]	5940	8367	16576	13516	4682
R_{int}	0.0357	0.0297	0.0313	0.0314	0.0507
Flack parameter	—	—	0.058(3)	—	—
parameters / restraints	463 / 0	475 / 0	1109 / 13	863 / 0	325 / 0
GOF on F^2	0.807	0.982	0.860	1.006	0.945
R_1 / wR_2 [I>2 $\sigma(I)$]	0.0353 / 0.0529	0.0178 / 0.0344	0.0237 / 0.0384	0.0267 / 0.0530	0.0243 / 0.0470
R_1 / wR_2 (all data)	0.0549 / 0.0548	0.0230 / 0.0349	0.0295 / 0.0387	0.0369 / 0.0561	0.0382 / 0.0485
max / min $\Delta\rho$[eÅ^{-3}]	2.006 / –1.743	1.717 / –0.953	1.171 / –0.810	0.129 / –0.793	1.821 / –1.708

9 DFT studies and AIM analyses

DFT optimizations were performed using the Gaussian 09 program[6] (functional, B3LYP[7], mixed basis sets: Hg, cc-pVTZ-PP[8] with the Stuttgart relativistic small core ECP;[9] P/Fe/As, 6-311++G**;[10] F, 6-31G(d');[11] H/C, 6-31G[12]) The AIM analyses were performed with the AIMAll[13] program using the wavefunction files generated from a single point energy calculation at the experimentally determined solid state geometry. XYZ plots of compounds **4** and **5** featuring all bond critical points found between **1** and **3** and **2** and **3**, respectively, as well as tables of the features of the electron distribution function as these critical points are shown below.

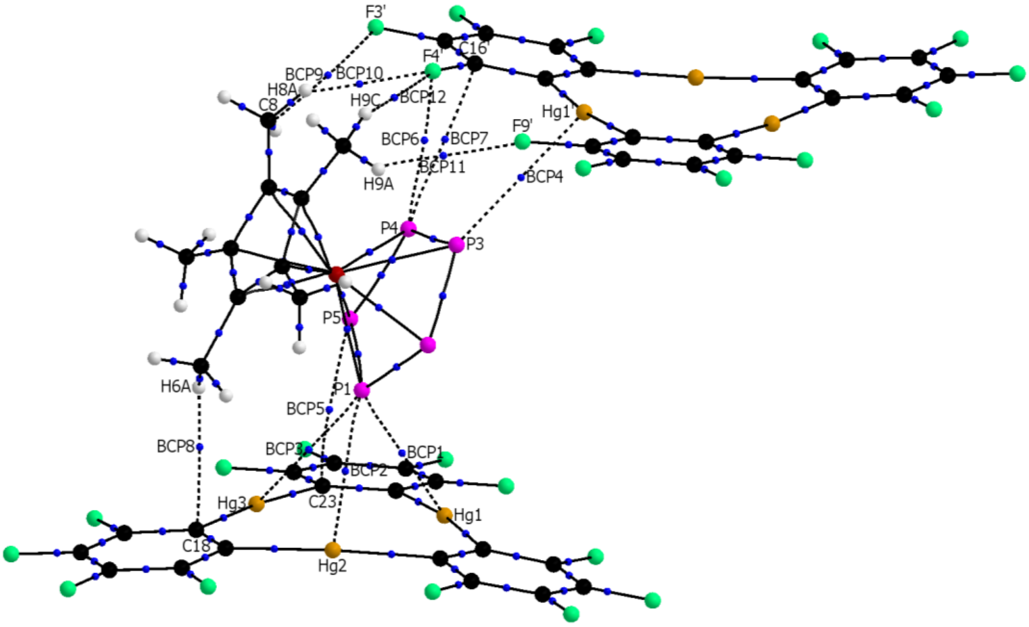

Figure 3. XYZ plot of compound 4, featuring all bond critical points found between the units of 2 and 3.

Table 6. Calculated features of the electron density distribution at the bond critical points between 1 and 3 in compound 4.

BCP No. (A-B)	*d*(A-BCP) (Å)	*d*(B-BCP) (Å)	$\rho(r_{BCP})$ (e Å^{-3})	$\nabla^2\rho(r_{BCP})$ (e Å^{-5})	$H(r_{BCP})/\rho(r_{BCP})$ (E_h e^{-1})	$G(r_{BCP})/\rho(r_{BCP})$ (E_h e^{-1})	ε
1(Hg1-P1)	1.657	1.630	0.105	0.876	0.012	0.570	0.048
2(Hg2-P1)	1.664	1.696	0.101	0.835	0.020	0.553	0.046
3(Hg3-P1)	1.754	1.776	0.072	0.620	0.055	0.546	0.046
4(Hg1'-P3)	1.737	1.789	0.072	0.622	0.065	0.542	0.051
5(P5-C23)	1.965	1.820	0.033	0.328	0.142	0.551	8.215
6(P4-F4')	1.808	1.486	0.042	0.678	0.140	0.845	1.283
7(P4-C16')	1.849	1.572	0.050	0.533	0.133	0.613	0.132
8(C18-H6A)	3.238	2.213	0.038	0.453	0.192	0.631	0.501
9(C8-F3')	3.457	3.084	0.018	0.342	0.357	0.892	1.923
10(H8A-F4')	1.982	2.697	0.049	0.864	0.232	1.000	0.026
11(H9A-F9')	2.429	3.010	0.017	0.335	0.384	0.961	0.033
12(H9C-F4')	2.065	2.734	0.037	0.692	0.272	1.036	0.052

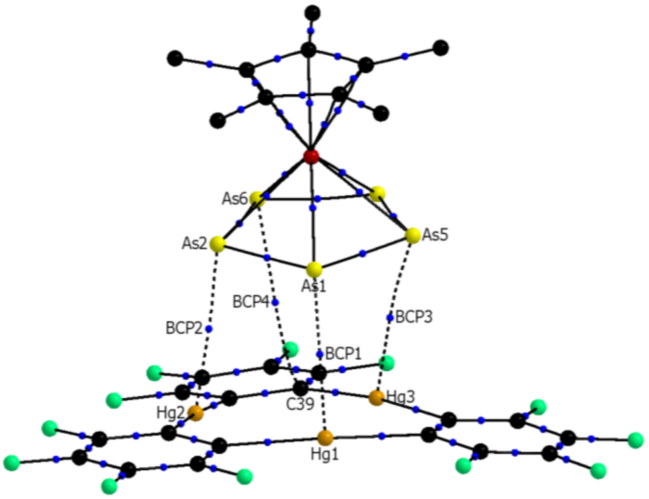

Figure 4. XYZ plot of compound 5, featuring all bond critical points found between the units of 2 and 3.

Table 7. Calculated features of the electron density distribution at the bond critical points between 2 and 3 in compound 5.

BCP No. (A-B)	d(A-BCP) (Å)	d(B-BCP) (Å)	$\rho(r_{BCP})$ (e Å^{-3})	$\nabla^2\rho(r_{BCP})$ (e Å^{-5})	$H(r_{BCP})/\rho(r_{BCP})$ (E_h e^{-1})	$G(r_{BCP})/\rho(r_{BCP})$ (E_h e^{-1})	ε
1(Hg1-As1)	1.698	1.707	0.091	0.757	0.044	0.540	0.031
2(Hg2-As2)	1.654	1.648	0.109	0.885	0.018	0.524	0.052
3(Hg3-As5)	1.695	1.731	0.096	0.762	0.027	0.549	0.344
4(As3-C18)	2.024	1.771	0.036	0.325	0.111	0.518	4.005

10 Hirshfeld surface analyses

In order to further investigate the present interactions in the solid state a detailed Hirshfeld surface analysis[14] of the mercury containing compounds (**4**, **5**, **7a-c**) was performed using the free of charge crystal explorer software.[15] After some general considerations we will present representations of all discussed Hirshfeld surfaces on the following pages describing some highlighted features. Finally we will conclude the discussion with some selected fingerprint plots.

10.1 General considerations:

All mercury containing compounds contain the same Lewis acid $[(o\text{-}HgC_6F_4)_3]$ (**3**). Therefore, a detailed discussion of the Hirshfeld surface of **3** in these compounds (**4**, **5**, **7a-c**) is presented here. Since the Lewis acid **3** has the characteristic of an almost planar geometry it is possible to easily distinguish two faces of the molecule. To simplify the following discussion we define the side which shows an interaction with either P or As atoms as the front while the opposite side is defined as the back (see scheme 3).

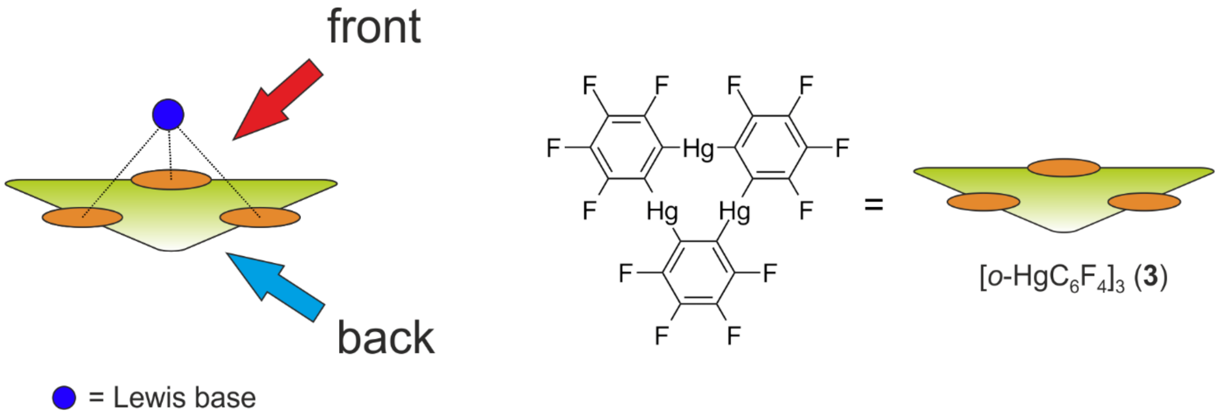

Scheme 3. Definition of front and back side of the planar Lewis acid 3.

10.2 d_{norm} values and the van der Waals radii

The d_{norm} values (depicted in figure 6-11 a) + b)) for Hirshfeld surfaces were defined[14a] to describe intermolecular contacts in normalized contact distances which are based on the van der Waals radii (vdW) of the involved atoms. The authors designed this very useful representation in a fashion, that: *“d_{norm} ... is displayed using a red-white-blue colour scheme, where red highlights shorter contacts, white is used for contacts around the vdW separation, and blue is for longer contacts.”*[14a] (page 3814, right column) This visual aid for close contacts is based on the vdW radii (for P 1.80 Å, As 1.85 Å and Hg 1.55 Å) which are also used by the CCDC and taken from the literature.[16] However, the author of this report states: *“the aforementioned metal radii are substantially smaller than predicted from ionization potentials ... It is not certain, therefore, how best to estimate the van der Waals radii of metals in metal organic compounds.”*[16] (page 448, right column) In the main text of this publication we state: *“The van der Waals (vdW) radius of Hg in different compounds is discussed in the literature with reported values ranging from 1.7 Å up to 2.2 Å*[17] *In the following discussion the shortest value of 1.7 Å is taking as a reference.”* The vdW radii of P (1.9) and As (2.0) for our discussion are adopted from an established inorganic textbook (HoWi).[18]

Therefore, the sum of the vdW radii from the crystal explorer software[15] (3.35 for Hg-P and 3.40 for Hg-As) differ from our estimates (3.6 for Hg-P and 3.7 for Hg-As). As a result the following representations of the d_{norm} values on the Hirshfeld surfaces (fig 6-11 a) clearly show close contacts of Hg to P and As atoms in the center of the molecule but these are unfortunately not highlighted as strongly as some close contacts (F-F and F-H for example) on the periphery.

10.3 Hirshfeld surface of compound 4

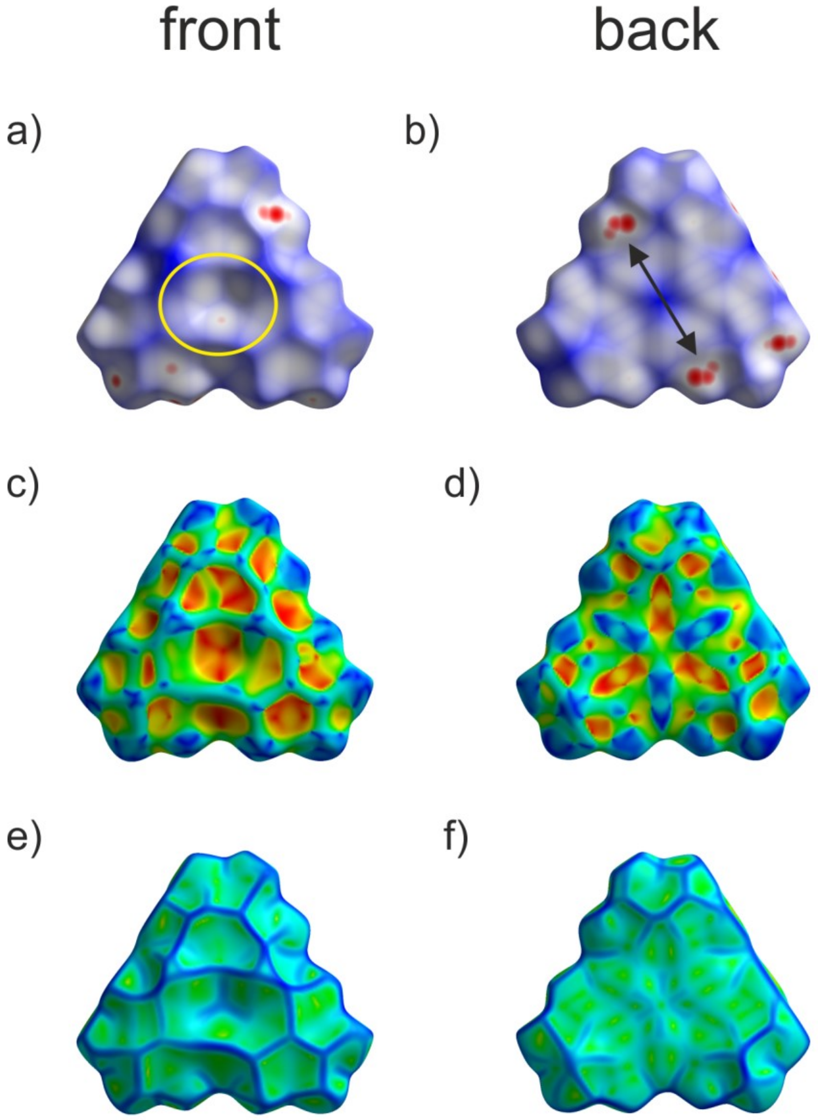

Figure 5. Representation of the Hirshfeld surface of the front (left) and the back (right) of the planar Lewis acid 3 in the compound [(Cp*FeP$_5$)•(3)] (4). The first row shows the *d*norm values, while the second row shows the shape index values and the third row shows the curvedness, respectively.

When looking at the front side of the molecule, one can see a distinctive indentation in the center highlighted in yellow which arises from three short contacts of one P atom to the three mercury atoms (white to red spots). This close approximation is also clearly visible as a red region in the shape index (c) and the three connected blue lines in the curvedness (e). In contrast, the back side of the Hirshfeld surface is flat which arises of a face to face arrangement of two molecules of **3** in the crystal lattice (by an inversion center which is situated directly above the center of the molecule). This can clearly be seen by the shape index (d) which shows self-complementary surface areas around the center of the molecule. In (b) two corresponding close contact regions are highlighted by an arrow.

10.4 Hirshfeld surface of compound 5

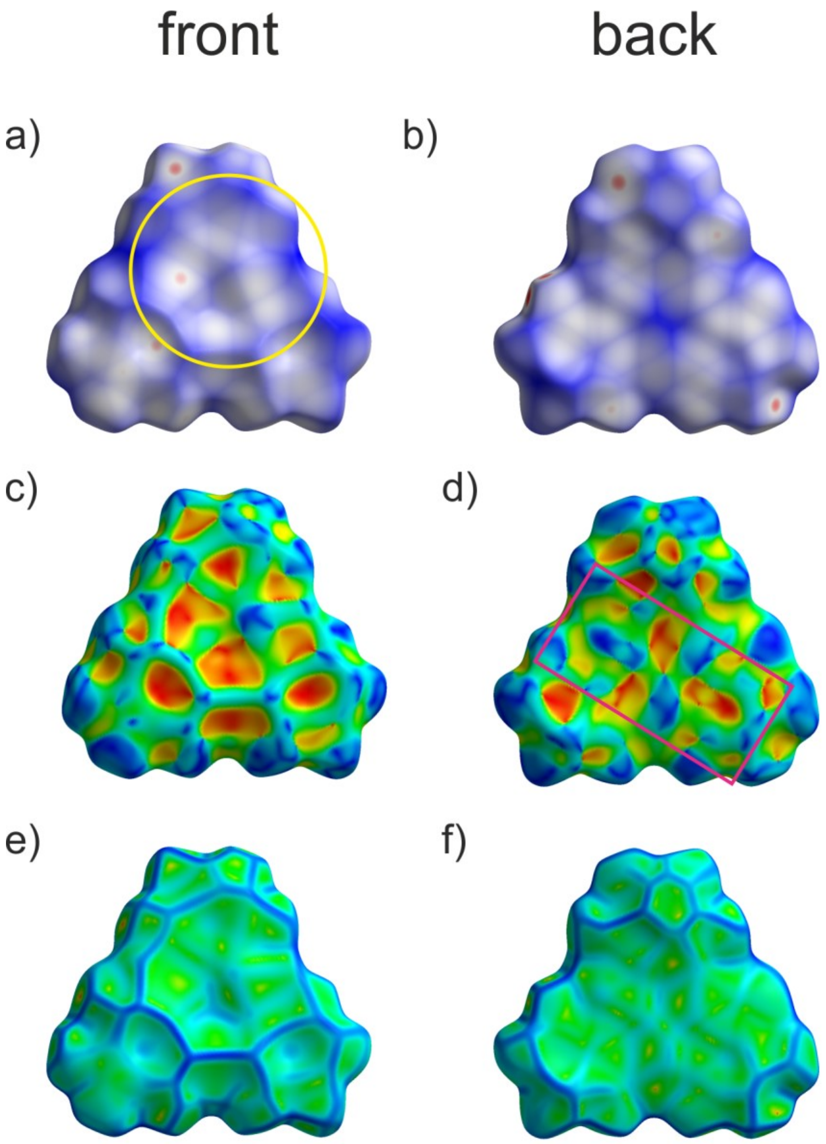

Figure 6. Representation of the Hirshfeld surface of the front (left) and the back (right) of the planar Lewis acid 3 in the compound [(Cp*FeAs$_5$)•(3)] (5). The first row shows the *d*norm values, while the second row shows the shape index values and the third row shows the curvedness, respectively.

When looking at the front of the molecule in (a) one can also see a shallow indentation in the center of the molecule like it was found for compound **4** (compare fig. 6 a), but this time it is not as pronounced. In this compound the *cyclo*-As$_5$ complex [Cp*Fe(η^5-As)$_5$] shows contacts to the front side of the Lewis acid **3** by all five As atoms resembling an almost face to face assembly highlighted in yellow. The fact that the Hirshfeld surface is greatly influenced by the five-membered As ring can be seen even more clearly when looking at the shape index (c) which exhibits five red spots or the curvedness (e) which shows a relatively smooth surface in the contact area.

The back side (b) of the molecule is flat. The shape index (d) shows large self-complementary surface regions highlighted in purple which reveal a face to face arrangement of two molecules of **3** by an inversion center which is situated slightly below the center of the molecule in this representation.

10.5 Hirshfeld surface of compound 7a

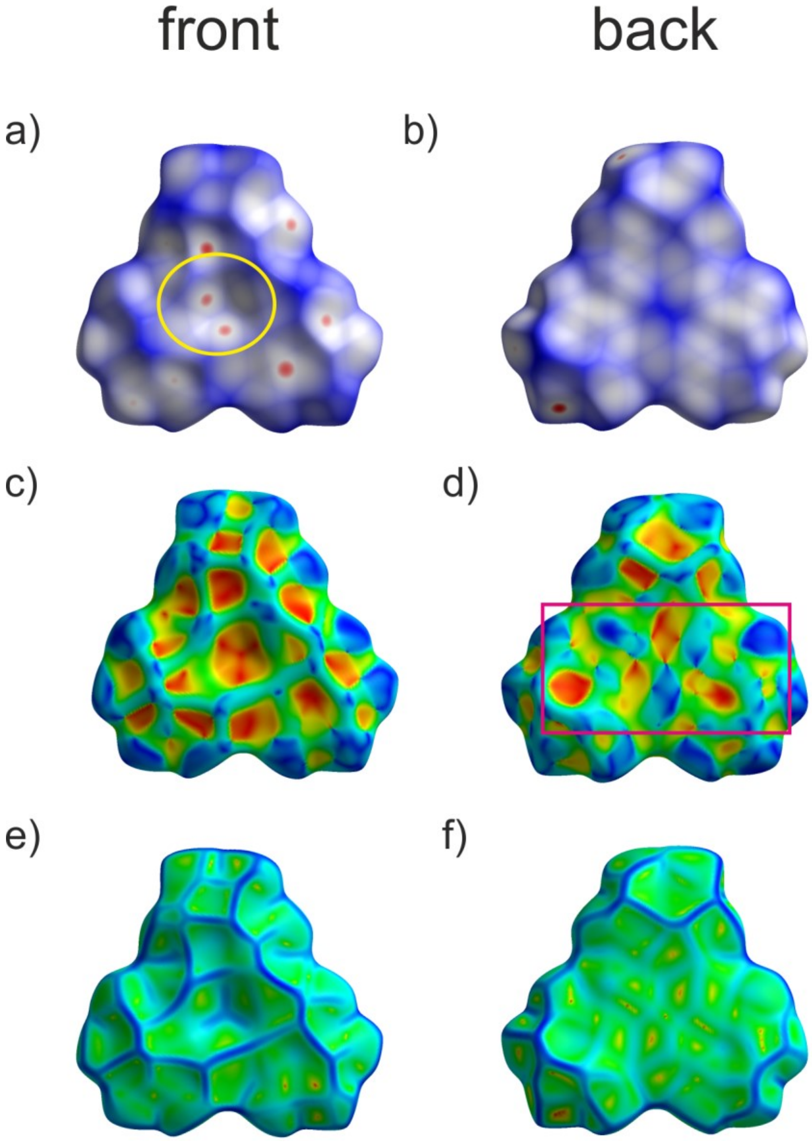

Figure 7. Representation of the Hirshfeld surface of the front (left) and the back (right) of the planar Lewis acid 3 in the compound [(Cp'FeP$_5$)•(3)] (7a). The first row shows the *d*norm values, while the second row shows the shape index values and the third row shows the curvedness, respectively.

The Hirshfeld surface of the Lewis acid **3** in the compound **7a** exhibits features which are very reminiscent of the compound **4** (compare fig. 6). Namely, a distinctive indentation in the center of the front side highlighted in yellow showing three contacts and a flat back side with large self-complementary surface areas.

10.6 Hirshfeld surface of compound 7b

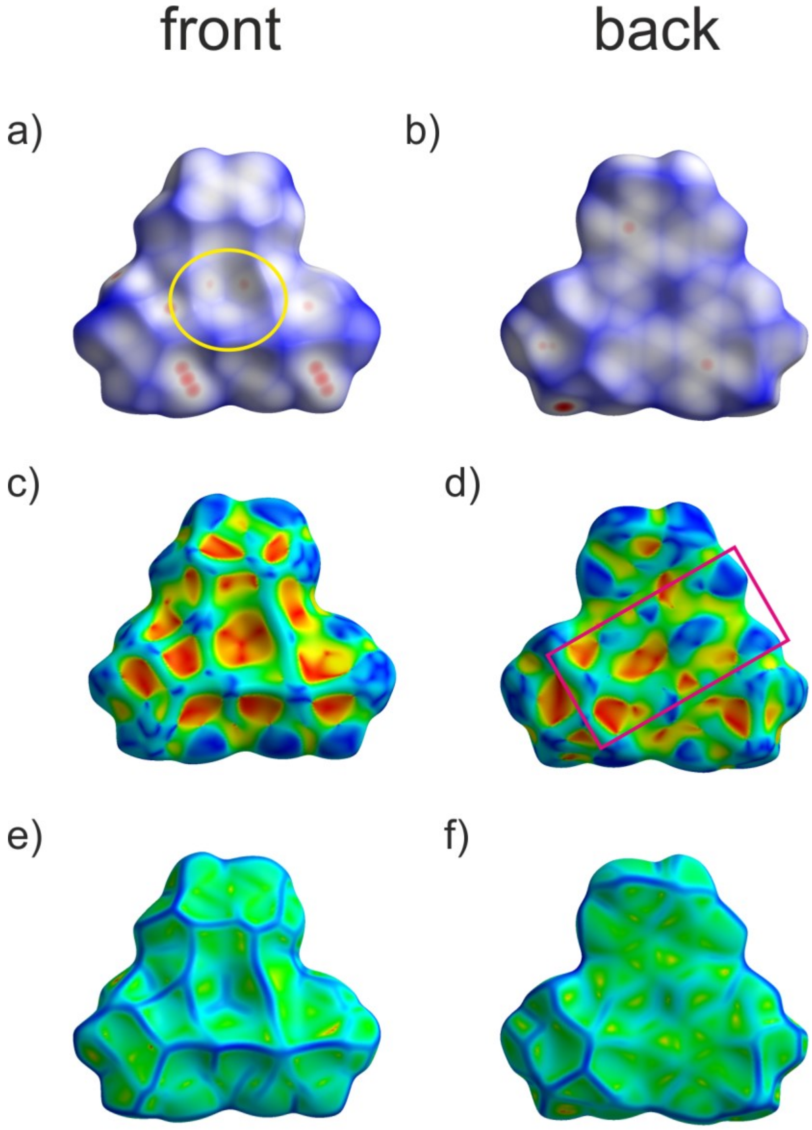

Figure 8. Representation of the Hirshfeld surface of the front (left) and the back (right) of the planar Lewis acid 3 in the compound [(Cp''FeP$_5$)•(3)] (7b). The first row shows the *d*norm values, while the second row shows the shape index values and the third row shows the curvedness, respectively.

The Hirshfeld surface of the Lewis acid **3** in the compound **7b** is closely related to the one found in compound **7a** (compare fig. 8) and also exhibits features which are very reminiscent of the compound **4** (compare fig. 6). Namely, a distinctive indentation in the center of the front side highlighted in yellow showing three contacts and a flat back side with large self-complementary surface areas.

10.7 Hirshfeld surface of compound 7c

The compound **7c** crystallizes with two independent molecules of the Lewis acid **3** in the asymmetric unit, but these show very similar environments. Therefore, the Hirshfeld surfaces for both molecules are presented separately, but the features will be discussed together.

Molecule 1:

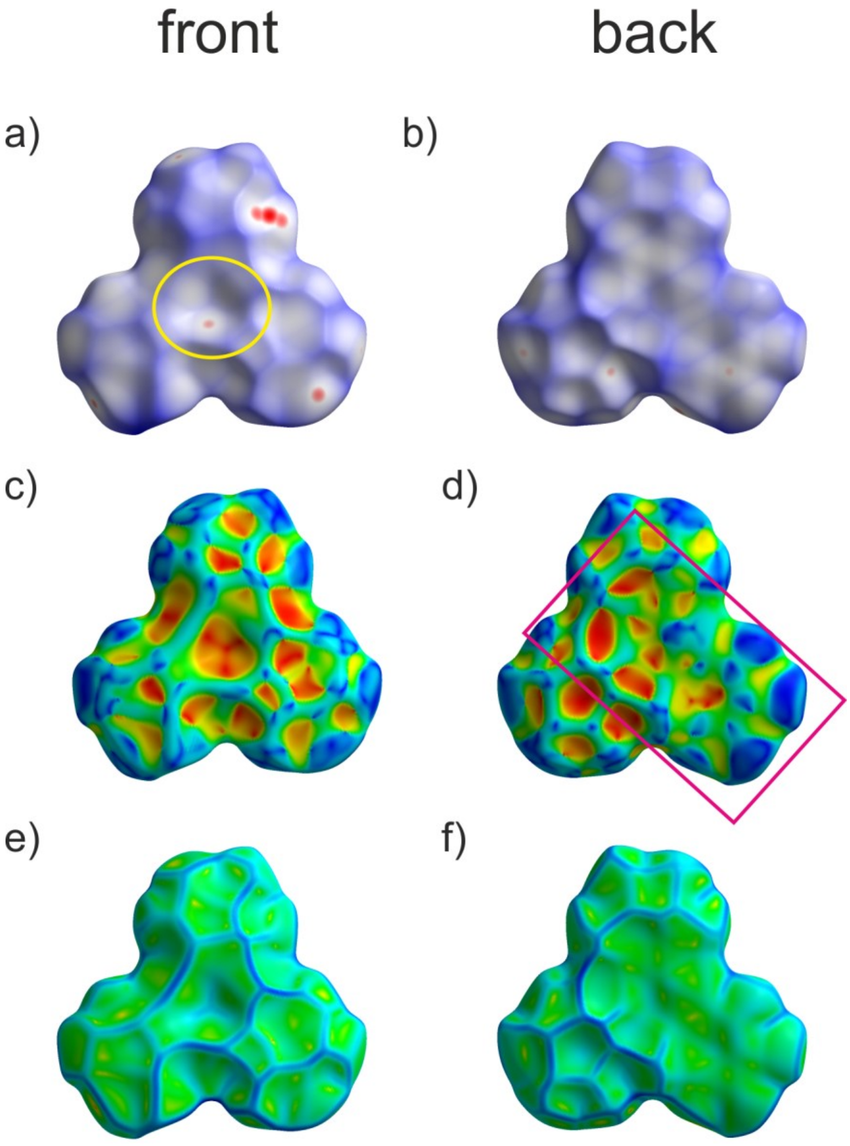

Figure 9. Representation of the Hirshfeld surface of the front (left) and the back (right) of molecule 1 in the compound [(Cp'''FeP$_5$)•(3)] (7c). The first row shows the *d*norm values, while the second row shows the shape index values and the third row shows the curvedness, respectively.

Molecule 2:

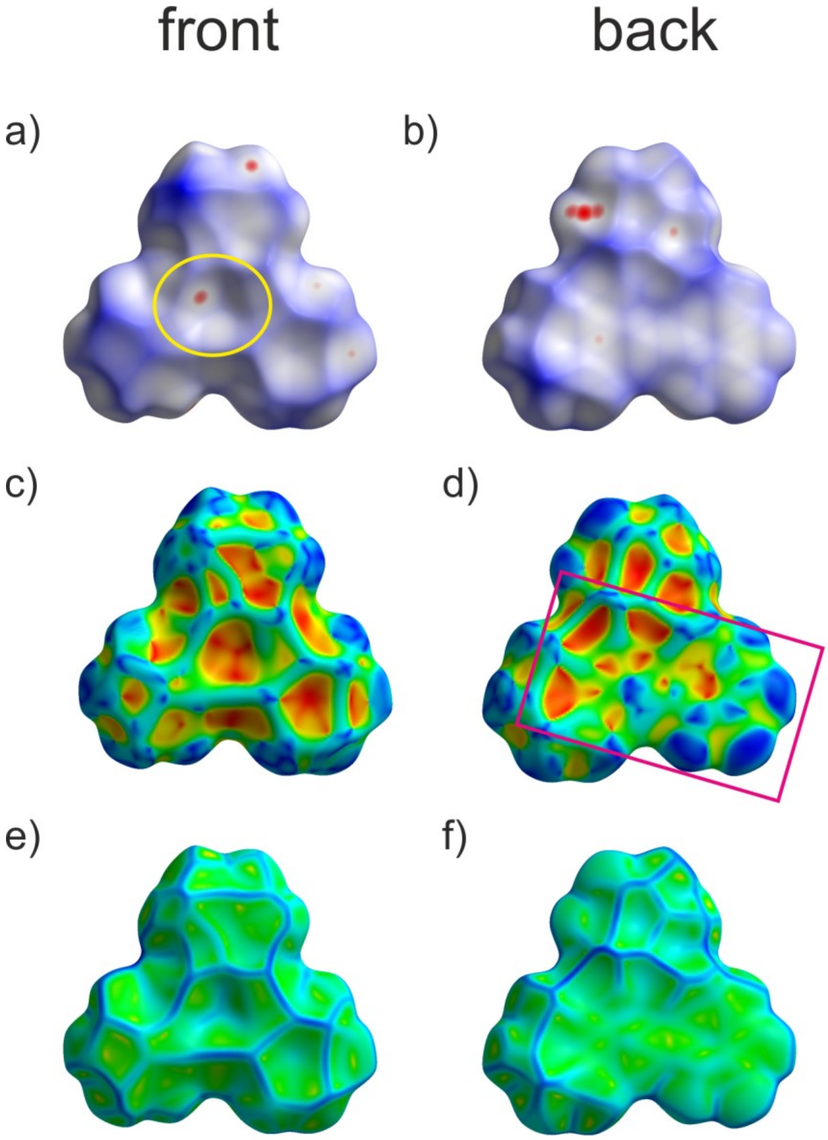

Figure 10. Representation of the Hirshfeld surface of the front (left) and the back (right) of molecule 2 in the compound [(Cp'''FeP$_5$)•(3)] (7c). The first row shows the *d*norm values, while the second row shows the shape index values and the third row shows the curvedness, respectively.

The Hirshfeld surfaces of the Lewis acid **3** in the compound **7c** exhibit features which are very reminiscent of the compounds **4**, **7a** and **7b** (compare fig. 6, 8 and 9). Namely, a distinctive indentation in the center of the front side highlighted in yellow showing three contacts and a flat back side. The only difference is the orientation of the next planar Lewis acid **3** in respect to the center of the molecule. In this case the next molecule of **3** is not created via an inversion center in the solid state but is an independent molecule (molecule 1 on top of molecule 2 and vice versa). Nevertheless, since the environment of the two molecules is very similar, their Hirshfeld surfaces show very similar features. When looking at figure 10 and 11 (d) the purple rectangles highlight surface areas which show almost complementary shape indexes although they are not self-complementary.

11 Fingerprint plots of the compounds 4, 5 and 7a-c

On the following pages we present selected fingerprint plots of the planar Lewis acid **3** in the mercury containing coordination compounds **4**, **5** and **7a-c**. These plots visually present intermolecular contacts in d_i-d_e pairs which describe the distances of the nearest nuclei inside or outside the Hirsheld surface to one particular point on the surface. The plots are color coded to show the relative frequency of specific d_i-d_e pairs, but they do not take different atom sizes into account. Therefore, short Hg-P distances will be found in different regions than short C-H distances. The surface of the investigated Lewis acid **3** in all compounds roughly consists of 11.5% contribution from Hg atoms, 63% from F atoms and 25.5% from C atoms.

11.1 Decomposed fingerprint plots of compound 4

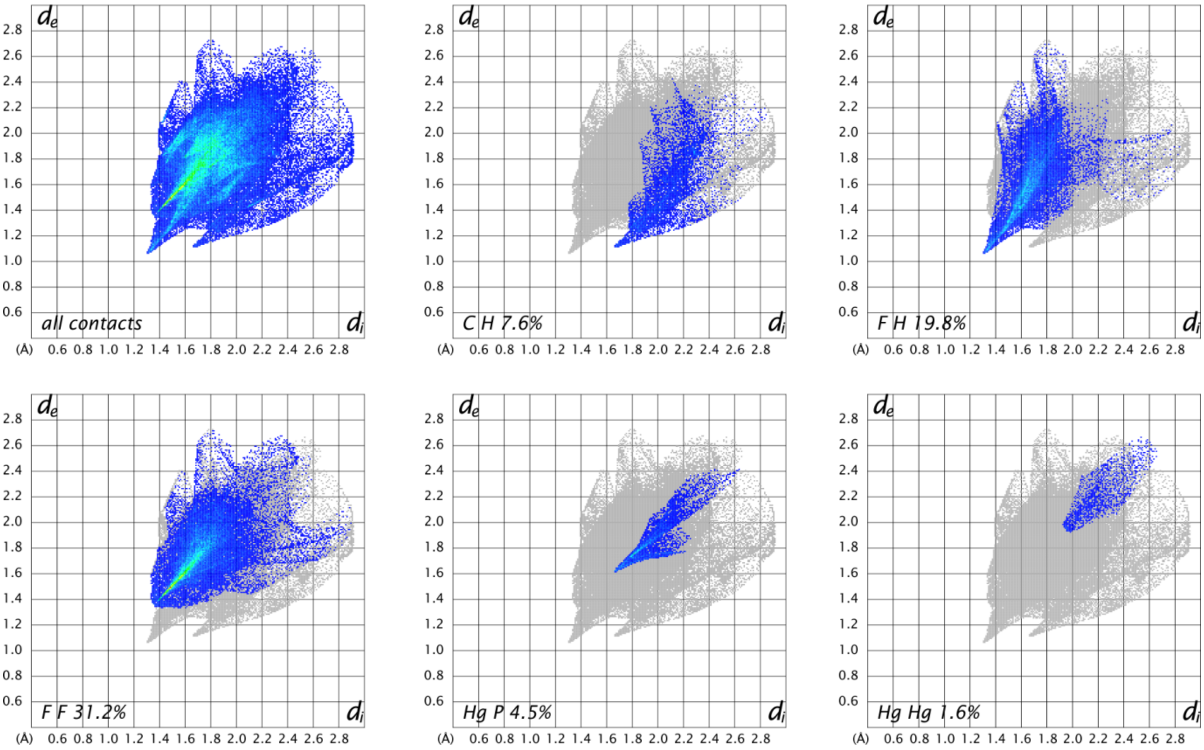

Figure 11. Selected fingerprint plots of compound 4.

The decomposed fingerprint plots of compound **4** reveal that the two tips at the bottom of the plot representing the shortest contacts arise from F-H and C-H contacts. While F-F contacts contribute the major part of contacts, Hg-Hg contacts only contribute 1.6% with rather long intermolecular distances. The Hg-P contacts contribute 4.5% with some of the contacts in a short region for these atoms.

11.2 Decomposed fingerprint plots of compound 5

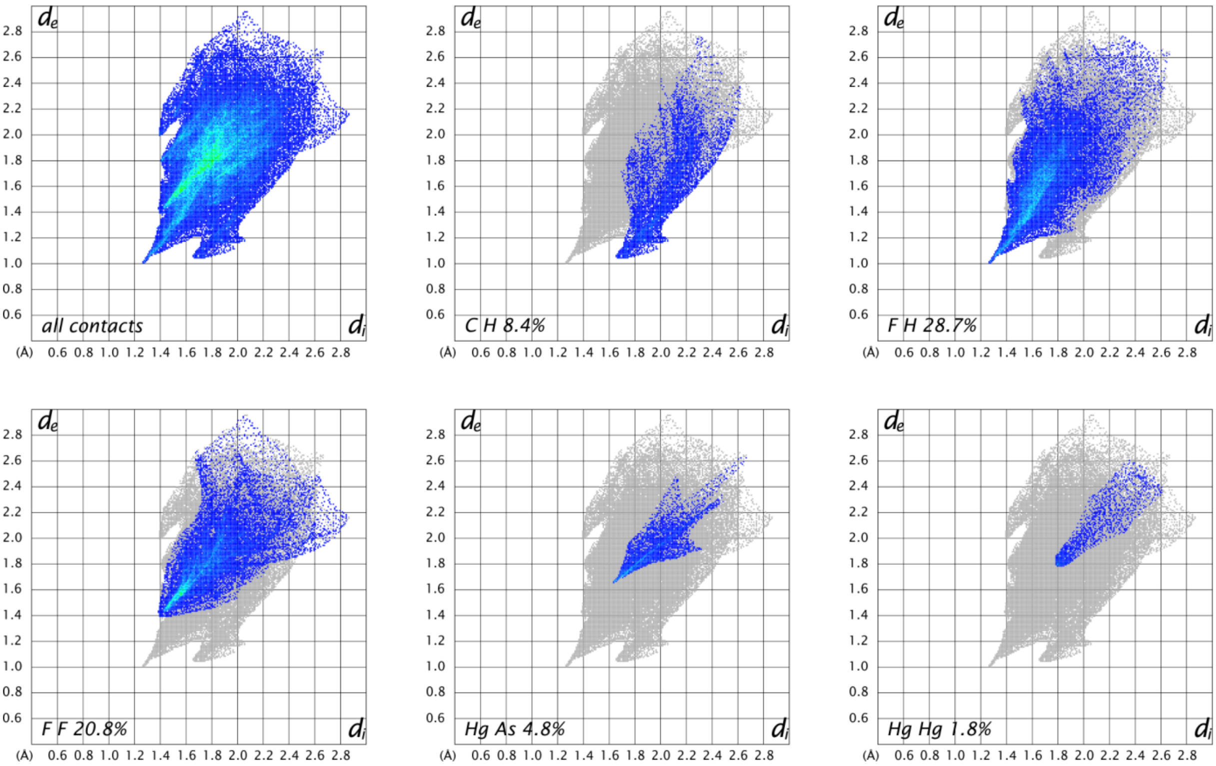

Figure 12. Selected fingerprint plots of compound 5.

The decomposed fingerprint plots of compound **5** exhibit some similar features like it was found for compound **4**. The closest contact regions arise from F-H and C-H contacts. While this time the F-H contacts contribute the major part, there are still 20.8% of F-F contacts. Hg-Hg contacts only contribute 1.8% with intermolecular distances which are a little shorter than for compound 4. The Hg-As contacts contribute 4.8% with some of the contacts in a short region for these atoms.

11.3 Decomposed fingerprint plots of compound 7a

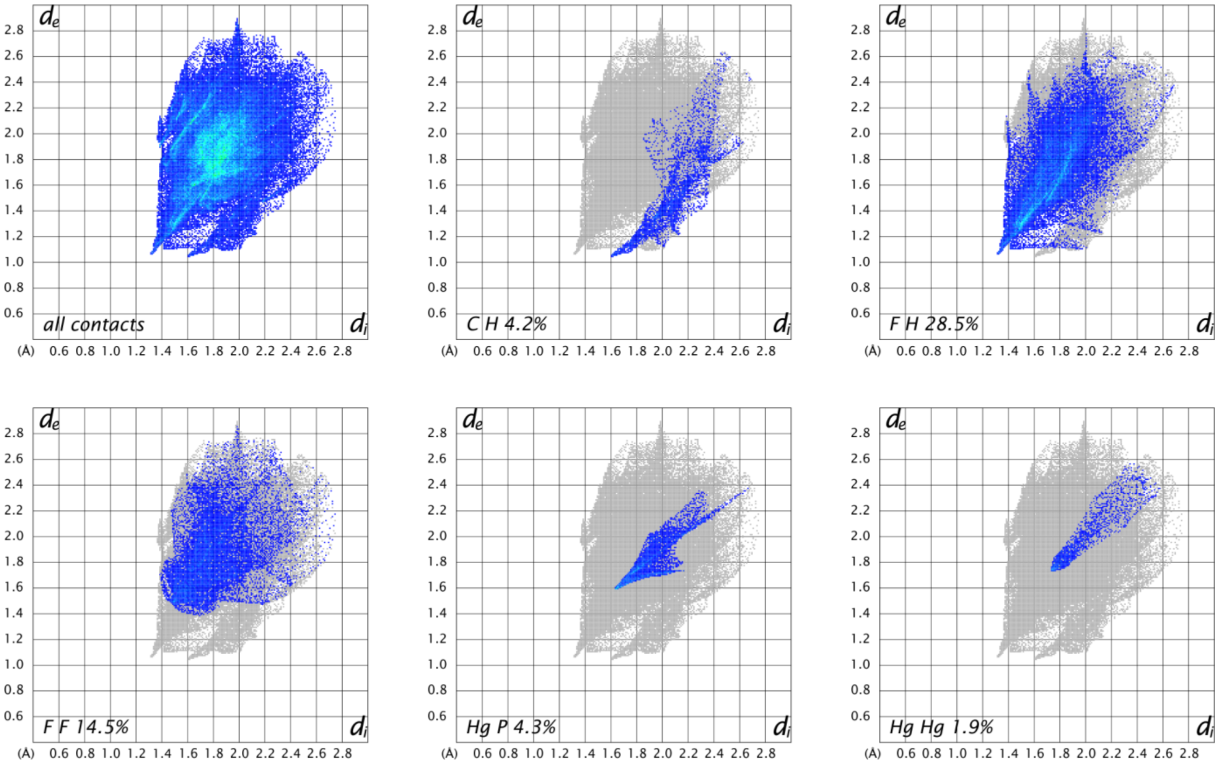

Figure 13. Selected fingerprint plots of compound 7a.

The decomposed fingerprint plots for this compound show similar features like the plots for compound **4** (compare fig. 12), except the majority of the contacts arises from F-H contacts instead of F-F contacts. The Hg-P contact area contributes 4.3% and is therefore almost unchanged compared to compound **4**.

11.4 Decomposed fingerprint plots of compound 7b

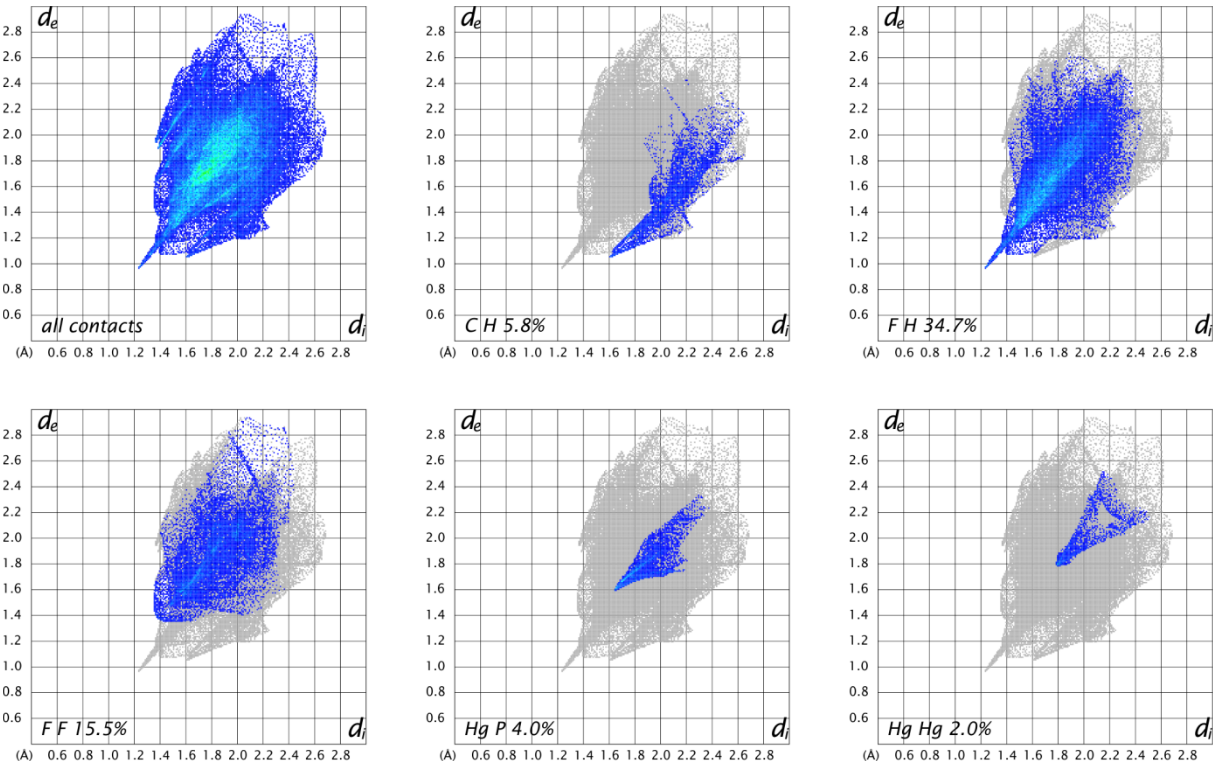

Figure 14. Selected fingerprint plots of compound 7b.

The decomposed fingerprint plots for compound **7b** show similar features like the plots for compound **4** (compare fig. 12), except the majority of the contacts arises from F-H contacts instead of F-F contacts and is even bigger than in compound **7a**. The Hg-P contact area contributes 4.0% and is therefore almost unchanged compared to compound **4**.

11.5 Decomposed fingerprint plots of compound 7c

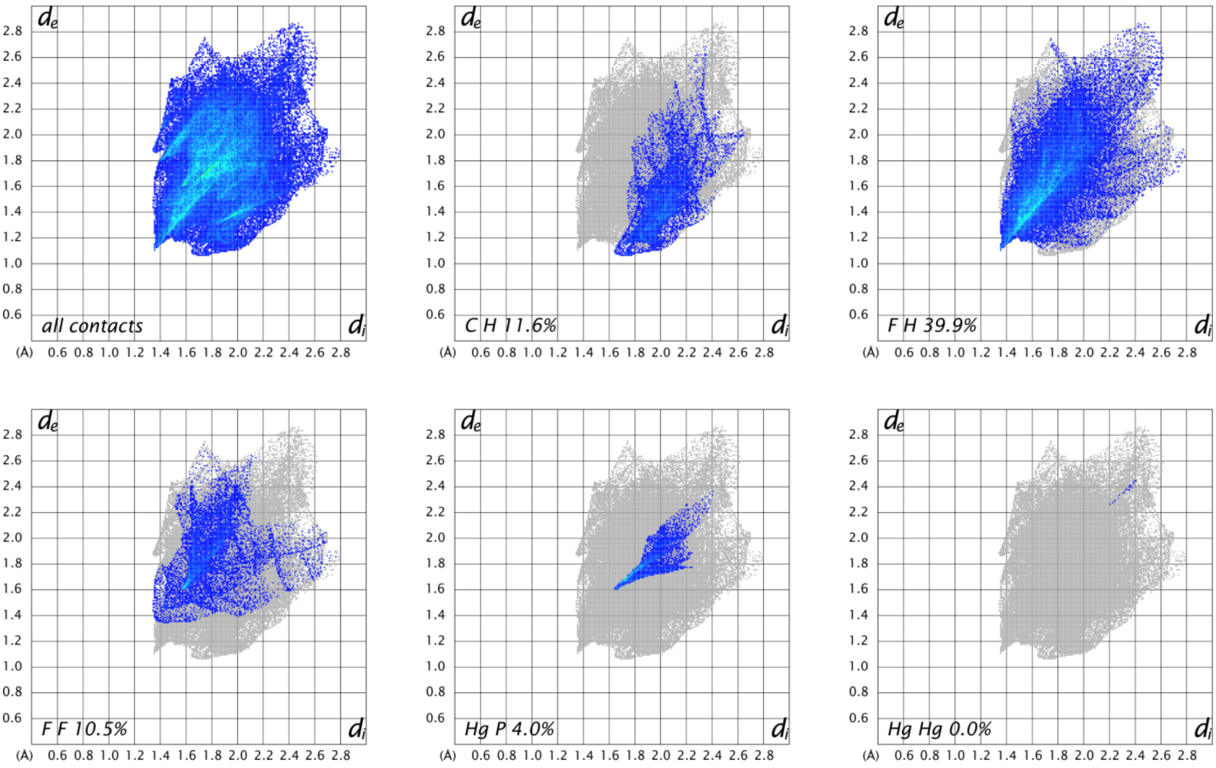

Figure 15. Selected fingerprint plots for compound 7c.

Since the Hirshfeld surface analysis of the two independent molecules in compound **7c** showed almost no difference, we only present the fingerprint plots for one molecule. The decomposed fingerprint show that the shortest contacts arise again from F-H and C-H contacts. The majority of the contacts arises from F-H contacts. The percentage of F-H contacts is the highest for all described compounds. This can easily be rationalized by the increasing size of the Cp ligand and the increasing hydrogen content of the P_5 sandwich complex. Nevertheless, the Hg-P contact area still contributes 4.0% and is therefore almost unchanged compared to compound **4**. No Hg-Hg contacts are present in this compound. This due to the fact, that different molecules of the planar Lewis acid **3** are not situated directly on each other (see figure 10 and 11 for an explanation).

References:

[1] a) O. J. Scherer, T. Brück, *Angew. Chem.* **1987**, *99*, 59-59; b) O. J. Scherer, T. Brück, *Angew. Chem. Int. Ed.* **1987**, *26*, 59-59; c) O. J. Scherer, C. Blath, G. Wolmershäuser, *J. Organomet. Chem.* **1990**, *387*, C21-C24; d) P. Sartori, A. Golloch, *Chem. Ber.* **1968**, *101*, 2004-2009.

[2] different versions, Agilent Technologies Ltd. (former Oxford Diffraction Ltd.), Oxford, UK.

[3] A. Altomare, M. C. Burla, M. Camalli, G. L. Cascarano, C. Giacovazzo, A. Guagliardi, A. G. G. Moliterni, G. Polidori, R. Spagna, *J. Appl. Cryst.* **1999**, *32*, 115-119.

[4] G. M. Sheldrick, *Acta Cryst. A* **2008**, *64*, 112-122.

[5] E. Keller, Freiburg, **1997**.

[6] M. J. Frisch, G. W. Trucks, H. B. Schlegel, G. E. Scuseria, M. A. Robb, J. R. Cheeseman, G. Scalmani, V. Barone, B. Mennucci, G. A. Petersson, H. Nakatsuji, M. Caricato, X. Li, H. P. Hratchian, A. F. Izmaylov, J. Bloino, G. Zheng, J. L. Sonnenberg, M. Hada, M. Ehara, K. Toyota, R. Fukuda, J. Hasegawa, M. Ishida, T.

Nakajima, Y. Honda, O. Kitao, H. Nakai, T. Vreven, J. A. Montgomery Jr., J. E. Peralta, F. Ogliaro, M. J. Bearpark, J. Heyd, E. N. Brothers, K. N. Kudin, V. N. Staroverov, R. Kobayashi, J. Normand, K. Raghavachari, A. P. Rendell, J. C. Burant, S. S. Iyengar, J. Tomasi, M. Cossi, N. Rega, N. J. Millam, M. Klene, J. E. Knox, J. B. Cross, V. Bakken, C. Adamo, J. Jaramillo, R. Gomperts, R. E. Stratmann, O. Yazyev, A. J. Austin, R. Cammi, C. Pomelli, J. W. Ochterski, R. L. Martin, K. Morokuma, V. G. Zakrzewski, G. A. Voth, P. Salvador, J. J. Dannenberg, S. Dapprich, A. D. Daniels, Ö. Farkas, J. B. Foresman, J. V. Ortiz, J. Cioslowski, D. J. Fox, Gaussian, Inc., Wallingford, CT, USA, **2009**.

[7] a) J. P. Perdew, W. Yue, *Phys. Rev. B,* **1986**, *33*, 8800-8802; b) A. D. Becke, *J. Chem. Phys.* **1993**, *98*, 5648-5652.

[8] K. A. Peterson, C. Puzzarini, *Theor Chem Acc* **2005**, *114*, 283-296.

[9] D. Figgen, G. Rauhut, M. Dolg, H. Stoll, *Chem. Phys.* **2005**, *311*, 227-244.

[10] a) A. J. H. Wachters, *J. Chem. Phys.* **1970**, *52*, 1033-1036; b) P. J. Hay, *J. Chem. Phys.* **1977**, *66*, 4377-4384.

[11] a) G. A. Petersson, A. Bennett, T. G. Tensfeldt, M. A. Al ‐ Laham, W. A. Shirley, J. Mantzaris, *J. Chem. Phys.* **1988**, *89*, 2193-2218; bG. A. Petersson, M. A. Al ‐ Laham, *J. Chem. Phys.* **1991**, *94*, 6081-6090.

[12] R. Ditchfield, W. J. Hehre, J. A. Pople, *J. Chem. Phys.* **1971**, *54*, 724-728.

[13] T. A. Keith, TK Gristmill Software, Overland Park KS, USA, **2014**.

[14] a) J. J. McKinnon, D. Jayatilaka and M. A. Spackman, *Chem. Commun.*, **2007**, 3814-3816; b) J. J. McKinnon, A. S. Mitchell and M. A. Spackman, *Chem. Eur. J.*, **1998**, *4*, 2136-2141; c) M. A. Spackman and D. Jayatilaka, *Crystengcomm*, **2009**, *11*, 19-32; d) M. A. Spackman, *Phys. Scr.*, **2013**, *87*, 048103.

[15] www.hirshfeldsurface.net

[16] A. Bondi, *J. Phys. Chem.*, **1964**, *68*, 441–452.

[17] a) A. J. Canty and G. B. Deacon, *Inorg. Chim. Acta*, **1980**, *45*, L225-L227. b) S. S. Batsanov, *J. Chem. Soc., Dalton Trans.*, **1998**, 1541-1546. c) P. Pyykko and M. Straka, *PCCP*, **2000**, *2*, 2489-2493. d) K. R. Flower, V. J. Howard, S. Naguthney, R. G. Pritchard, J. E. Warren and A. T. McGown, *Inorg. Chem.*, **2002**, *41*, 1907-1912.

[18] A. F. Holleman, E. Wiberg and N. Wiberg, *Lehrbuch der Anorganischen Chemie*, Walter de Gruyter, Berlin, **2007**.